# Nucleosome interactions in chromatin: Fiber stiffening and hairpin formation

Boris Mergell,[1,*] Ralf Everaers,[2,†] and Helmut Schiessel[1,‡]
[1]*Max-Planck-Institut für Polymerforschung, Postfach 3148, D-55021 Mainz, Germany*
[2]*Max-Planck-Institut für die Physik komplexer Systeme, Nöthnitzer Strasse 38, D-01187 Dresden, Germany*
(Received 11 November 2003; revised manuscript received 22 April 2004; published 29 July 2004)

We use Monte Carlo simulations to study attractive and excluded volume interactions between nucleosome core particles in 30-nm chromatin fibers. The nucleosomes are treated as disklike objects having an excluded volume and short-range attraction modeled by a variant of the Gay-Berne potential. The nucleosomes are connected via bendable and twistable linker DNA in the crossed linker fashion. We investigate the influence of the nucleosomal excluded volume on the stiffness of the fiber. For parameter values that correspond to chicken erythrocyte chromatin, we find that the persistence length is governed to a large extent by that excluded volume whereas the soft linker backbone elasticity plays only a minor role. We further find that internucleosomal attraction can induce the formation of hairpin configurations. Tension-induced opening of such configurations into straight fibers manifests itself in a quasiplateau in the force-extension curve that resembles results from recent micromanipulation experiments. Such hairpins may play a role in the formation of higher-order structures in chromosomes like chromonema fibers.

DOI: 10.1103/PhysRevE.70.011915 PACS number(s): 87.14.Gg, 87.15.Aa, 87.15.La, 61.41.+e

## I. INTRODUCTION

DNA of all eucaryotic organisms is wrapped around millions of cylindrical protein spools, so-called histone octamers. Each complex has a radius of 5 nm and a height of 6 nm and—together with the stretch of linker DNA connecting to the next such spool—is called nucleosome, the basic unit of the chromatin complex [1]. In a next step of DNA compaction, the string of nucleosomes organizes itself into the chromatin fiber. For low-salt concentrations a "beads-on-a-string" structure is observed, sometimes referred to as the 10-nm fiber [2]. For higher salt concentrations ($>40$ mM) the fiber appears to thicken into a condensed structure with a diameter of roughly 30 nm [3]. The degree of compaction also depends strongly on the presence of linker histones. They cause the in- and outcoming DNA to form a short stemlike structure [4]. In the absence of linker histones the entry-exit angle of the in- and outcoming DNA is larger, leading to more open structures.

While the structure of the nucleosome core particle (the protein spool with the two turns of wrapped DNA) is known up to atomistic resolution [5], there is still considerable controversy about the details of the structure of the 30-nm chromatin fiber [1,6–9]. There are essentially two competing classes of models: (i) the solenoid models [2,10,11] and (ii) the zig-zag- or crossed-linker models [4,12,13]. In the solenoid models one assumes that the successive nucleosomes form a helix with the normal vectors of the protein spools (the axis of the superhelical wrapping path of the DNA) being perpendicular to the solenoidal axis. The entry-exit sides of the nucleosomal DNA face inward toward the solenoidal axis, and the linker DNA must bend in order to connect neighboring nucleosomes. In contrast the linker DNA in crossed-linker models remains straight and connects nucleosomes that sit on opposite sides of the fiber.

Chromatin fibers have been studied for various salt concentrations using electron cryo-microscopy [4,14], atomic force microscopy [15,16], neutron scattering, and scanning transmission electron microscopy [17]. Structural parameters, such as the mass density (number of nucleosomes per 11 nm) and the linker entry-exit angle, are measured to characterize the state of compaction. For low-salt concentrations all these studies support the picture of an open zig-zag-like fiber structure. Similarly the force-extension curves of single chromatin fibers measured under these conditions [18] (for a recent review see Ref. [19]) are in good agreement with the results from computer simulations [20] and analytical approaches [13,21,22] based on crossed-linker geometries of the fiber (for a recent review see Ref. [23]).

The situation is less clear at physiological salt concentrations. The internal structure of the dense 30-nm fiber could not yet be resolved despite enormous experimental efforts, especially x-ray diffraction studies (cf., Ref. [24] for a critical discussion). The interpretation of related studies on di- and trinucleosomes is also still controversial [8,14,25,26]. Even less is known about how chromatin folds into chromosomes on larger scales. Theories for the elastic properties of the DNA-linker backbone predict rather flexible fibers with persistence lengths on the order of 10–20 nm (compared to 50 nm for uncomplexed DNA). In contrast, Münkel and Langowski [27] and Wedemann and Langowski [28] have presented convincing evidence from experiments and simulations for rather large persistence length on the order of 300 nm. At the same time, the quasiplateau at 5 pN that Cui and Bustamante observed in their stretching experiments at physiological salt concentrations points to rather delicate features in the fiber structure (for comparison, the B-S transition in DNA is observed at a critical force of 65 pN [29]).

In the present paper we use computer simulations to study the consequence of internucleosome attractive and excluded

*Electronic address: mergell@mpip-mainz.mpg.de
†Electronic address: everaers@mpipks-dresden.mpg.de
‡Electronic address: heli@mpip-mainz.mpg.de

 

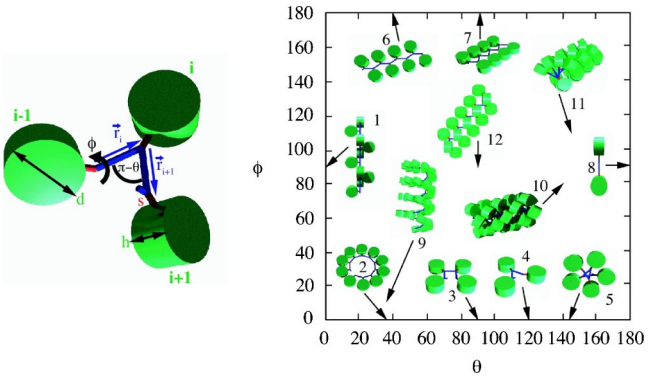


FIG. 1. Lhs: Portion of the model fiber including three nucleosomes (represented in this figure as green *cylinders* instead of ellipsoids to facilitate the identification of the nucleosome orientation) connected via stems (red) to the DNA linkers (blue). Also indicated are the two underlying angles: the deflection angle $\theta$ and the rotational angle $\phi$. Rhs: Examples of two-angle fibers with the arrows denoting their position in the $(\theta,\phi)$-plane.

volume interactions in dense crossed-linker fibers. Our chromatin fiber model is depicted on the left-hand side (lhs) of Fig. 1. We model the protein spools as ellipsoidal disks and assume that linker histones induce the in- and outcoming DNA to form stemlike structures [4]. Our opening and rotation angles $\pi-\theta$ and $\phi$ are compatible with experimentally observed values for the 30 nm fibers [4,30] (see the fiber "10" on the right-hand side (rhs) of Fig. 1). As a consequence, the *local* fiber geometry remains basically unchanged when we vary the strength of the attractive interaction. Local condensation-decondensation transitions in chromatin fibers [13,23] will be investigated in a forthcoming study [31].

With respect to the degree of coarse-graining of the nucleosome structure our model is comparable to the one employed by Katritch, Bustamante, and Olson [20]. The main difference is their use of quenched, randomly distributed $\phi$-angles along the chain. Since we are interested in rather generic features of the dense 30-nm fiber with a narrow distribution of linker lengths (and hence twist angles) [30], we focus on the ideal case of a constant $\phi$-angle for all linkers. Furthermore, we follow Wedemann and Langowski [28] in modeling the nucleosomes as ellipsoids (as opposed to spheres as in Ref. [20]) interacting via a Gay-Berne (GB) potential. However, we have not included Debye-Hückel interactions between different parts of the linker DNA [28], since the Debye-Hückel screening length is smaller than the diameter of the DNA double helix at physiological salt concentrations. As a consequence, intra- and inter-linker electrostatic interactions can be accounted for by renormalized bending rigidities [32] and opening angles $\pi-\theta$ [33], respectively.

Problematic for all attempts to model chromatin are the soft parts of the nucleosome. The charges on the linker histones H1/H5 and the histone tails are under biochemical control, allowing the cell to regulate the stem formation and the attractive interactions between nucleosomes [8,34]. While simulations investigating this "tail-bridging" effect [35,36] between nucleosomes are on the way [37], we prefer a generic nucleosome interaction potential to a model that neglects the tails, but accounts in detail for the surface charges on the nucleosome core [38]. Similarly, little is known about the stem structure (see the cryomicrographs in Ref. [4]), and for simplicity we have assumed that the short axis of the nucleosomal disk (the axis of the superhelical wrapping path) is oriented perpendicular to the plane defined by the in- and outgoing DNA linker.

The paper is organized as follows. Section II introduces our chromatin model and the methods used. We present our results for the mechanical fiber properties in Sec. III. Section IV provides a discussions of the observed hairpin structures and possible biological implications of our findings. Finally, we give a conclusion in Sec. V.

## II. MODEL AND METHODS

### A. Definition of the chromatin model

Our chromatin fiber model is depicted on the lhs of Fig. 1. We model the protein spools as ellipsoidal disks with a diameter of 10 nm and a height of 6 nm corresponding to the experimental values [5,39]. We assume that the in- and outcoming DNA are glued together in rigid stemlike structures that mimic the nucleosomal structures observed in the electron cryomicrographs in the presence of linker histones [4]. The stem portion is assumed to end 7 nm from the center of the corresponding protein spool. From this point on the entering and exiting linker DNA portions of length $B$ connect to the next nucleosomes.

The presence of a stem has to be taken into account when one calculates the length of the free linker DNA from the nucleosomal DNA repeat length, a number that varies not only from organism to organism, but even from tissue to tissue of the same organism [1]. It is known that 147 base pairs (bp) are closely associated with the protein spool wrapping the histone core in 1.65 turns [5]. We assume here that the presence of the linker histone forces the DNA to wrap two full turns corresponding to 177 bp. Together with the 2 -nm stem, this makes 189 bp that are associated with the core and linker histones. For instance, in the case of chicken erythrocyte chromatin the nucleosomal repeat length amounts to about 210 bp [1] so that there are roughly 21 bp, i.e., $B=7.14$ nm, of free linker DNA. In the following simulation runs, we will always use this value for $B$.

There are two angles that determine the fiber geometry: the deflection angle $\theta$ and the rotational angle $\phi$. The former angle characterizes the entry-exit angle $\pi-\theta$ of the linker DNA at the stem and the latter angle describes the rotational setting of the nucleosomal disks with respect to the DNA. Some example configurations are depicted on the rhs of Fig. 1 with the arrows pointing to their location in the $(\theta,\phi)$-space. Note that some configurations are forbidden because they would lead to overlapping nucleosomes; a systematic investigation of the boundary between allowed and forbidden structures will be provided in a forthcoming study [31].

In the present study we use a canonical value of $\theta=145°$ which has been estimated experimentally [4] at 80 -mM salt concentration. Having fixed $B$ and $\theta$ we have cho-

sen values of $\phi$ that lead to a reasonable nucleosome line density. Based on Eq. (78) in Ref. [23], we expect 6.5 nucleosomes per 11 nm for $\phi=100°$ and 6.1 nucleosomes per 11 nm for $\phi=110°$ compared to experimental estimates of 6–7 nucleosomes per 11 nm [4,17].

The only nonrigid elements in our model are the linker DNA portions. We discretize the linkers into four segments in order to allow for the bending and torsional deformations. To each segment $i$ we attach a local set of basis vectors $\{\mathbf{t}_i,\mathbf{n}_i,\mathbf{b}_i\}$ where $\mathbf{t}_i$ denotes the tangent vector, $\mathbf{n}_i$ the normal, and $\mathbf{b}_i$ the binormal vector. The elastic energy of the linkers is then described by

$$\frac{\mathcal{H}_{el}}{k_BT}=\frac{\tilde{l}_p}{2b}\sum_{i=1}^{4(N-1)+2}(\beta_i-\beta_{sp})^2+\frac{\tilde{l}_{Tw}}{2b}\sum_{i=1}^{4(N-1)+2}(\tau_i-\tau_{sp})^2, \quad (1)$$

where $\tilde{l}_p$ and $\tilde{l}_{Tw}$ are the DNA bending and twist persistence lengths, respectively, $N$ is the number of nucleosomes in our fiber, and $b$ denotes the segment length (i.e., $B=4b$). $\beta_i=\arccos(\mathbf{t}_i\cdot\mathbf{t}_{i+1})$ refers to the bending angle between two neighboring segments, and $\tau_i$ denotes the twist angle. The spontaneous bending angle $\beta_{sp}$ is equal to $\theta$ for those segment pairs, which are connected to a stem and is zero otherwise. $\tau_{sp}=\phi/3$ everywhere (except at the kink where $\tau_{sp}=0$) enforces the right-handed helicity of the DNA, which in turn gives rise for the fiber twist angle $\phi$.

The position and orientation of the nucleosomes is calculated from the linker positions with the help of a set of three orthonormal basis vectors $\{\mathbf{T}_i,\mathbf{N}_i,\mathbf{B}_i\}$. $\mathbf{N}_i$ is the normal vector perpendicular to the disk plane that we assume to be given by

$$\mathbf{N}_i=\frac{\vec{r}_i\times\vec{r}_{i+1}}{|\vec{r}_i\times\vec{r}_{i+1}|}. \quad (2)$$

Here the set $\{\vec{r}_i\}$ denotes the vectors that connect the stems of neighboring nucleosomes (see Fig. 1). $\mathbf{B}_i$ points from the tip of the stem toward the center of the nucleosomal disk, i.e.,

$$\mathbf{B}_i=\frac{\vec{r}_i-\vec{r}_{i+1}}{|\vec{r}_i-\vec{r}_{i+1}|}. \quad (3)$$

Finally, $\mathbf{T}_i$ is defined as

$$\mathbf{T}_i=\mathbf{N}_i\times\mathbf{B}_i. \quad (4)$$

For the interactions of the nucleosome core particles we use the same variant of the GB potential for ellipsoids of arbitrary shape [40,41] as in a recent study of a stacked-ellipsoid model of DNA [42]. Here we set the structure matrix {Eq. (15) in Ref. [42]} equal to

$$S=\begin{pmatrix}h/2 & 0 & 0\\ 0 & d/2 & 0\\ 0 & 0 & d/2\end{pmatrix}, \quad (5)$$

where $d=1.67h$ is the diameter of the nucleosome core particle with a canonical value for the core particle height of $h=6$ nm [5]. The effective distance of closest approach $h_{12}$ between two ellipsoids is calculated using Eqs. (17)–(19) in Ref. [42]. In cases where we study purely repulsive hard-core interactions, we reject all Monte Carlo moves leading to values $h_{12}<0$. In cases where we study attractive interactions, the distance-dependent part of the interaction potential Eq. (14) in Ref. [42] is given by a modified Lennard-Jones potential

$$U_r=4\epsilon_{GB}\left[\left(\frac{h}{h_{12}+h}\right)^{12}-\left(\frac{h}{h_{12}+h}\right)^{6}\right]. \quad (6)$$

The orientation-dependent parts are defined in Eqs. (20)–(25) in Ref. [42]. This parametrization of the GB potential leads to a preferred lateral spacing of about 7.0 nm and a vertical spacing of about 11.0 nm of the disks. The values are in good agreement with experimental results for columnar phases of nucleosome core particles [39]. In this paper we characterize the strength of the nucleosome-nucleosome attraction by the depth of the attractive well for two parallel disks $\epsilon=1.41\epsilon_{GB}$ instead of the prefactor $\epsilon_{GB}$ in Eq. (6).

### B. Methods

We use a Monte-Carlo scheme to simulate the chromatin fiber, which relies on the following three moves: (i) a local move where one randomly chooses a nucleosome that is rotated around an axis determined by two points on the in- and out-coming linker DNA by a small random angle, (ii) a nonlocal pivot move where a random segment point is chosen at which the shorter part of the chain is rotated around a random axis by a random angle, and (iii) a nonlocal crankshaft move where two random points along the DNA segments define the axis of rotation around which the inner part of the chain is rotated. The moves are accepted or rejected according to the Metropolis scheme [43].

We simulated either fibers with $N=50$ (simulations with applied stretching force) or $N=100$ nucleosomes corresponding to 10 and 20 kbp of DNA, respectively. The number of nucleosomes in pulling experiments by Cui and Bustamante [18] is on the same order ($\approx$300 nucleosomes). Each simulation run consists of 200 000 MC sweeps, where one sweep corresponds to $N_{DNA}$ trials with $N_{DNA}$ being the number of DNA segments. The amplitudes are chosen such that the acceptance rate equals approximately 50%. Every 20 sweeps we save a configuration. As initial conformation we used the relaxed ($T=0$) fiber structure. In order to determine the longest relaxation time $\tau_{corr}$ of the system, we measured the "time" correlation functions of the energy, mass density, end-to-end distance, and twist. We typically find that $\tau_{corr}\approx100$ MC sweeps. Note, however, that strong attractive interactions can cause a glasslike trapping of the fiber in local energy minima. As a consequence, only a limited range of attractive well depths can be studied meaningfully in simulations. In the present case, the simulation runs for $\epsilon=4k_BT$ were clearly nonergodic for low-stretching forces. In this case we averaged the results over 10 independent simulation runs.

The calculation of the elastic constants of the simulated fiber is performed as follows. First, we determine the fiber axis by calculating the centers of mass $\vec{c}_i=(1/N_c)\sum_{j=i}^{i+N_c}\vec{R}_j$ of groups of $N_c$ neighboring nucleosomes. $N_c$ is chosen to match approximately one or two helical turns. Then we calculate the autocorrelation function $\langle\mathbf{t}_i\cdot\mathbf{t}_j\rangle$ of the tangent vectors of the fiber axis

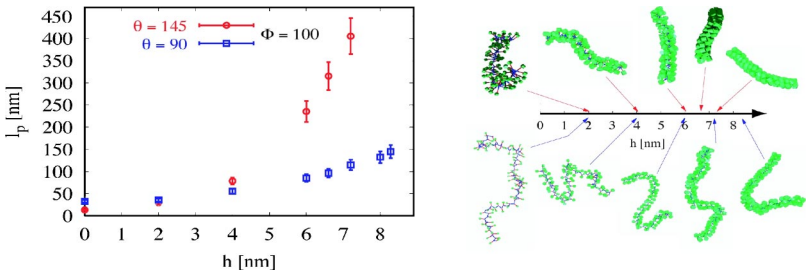


FIG. 2. Effect of the excluded volume interaction on the bending persistence length of the fiber for two deflection angles $\theta$ with $\phi=100°$ and $B=7.14$ nm. For a given linker length $B$, the fiber persistence length $l_p$ [nm] grows with increasing disk size. For very small disk sizes, the measured persistence lengths converge to the analytical result, Eq. (97) of Ref. [23]. On the rhs we show some snapshots of simulated fibers with varying disk sizes for $\theta=145°$ (top row) and $\theta=90°$ (bottom row).

$$\mathbf{t}_i = \frac{\vec{c}_{i+1} - \vec{c}_i}{|\vec{c}_{i+1} - \vec{c}_i|} \tag{7}$$

and extract the persistence length of the fiber $l_p$ from an exponential fit

$$\langle \mathbf{t}_i \cdot \mathbf{t}_j \rangle = \exp\left( - \frac{|i-j|b}{l_p} \right). \tag{8}$$

The stretching modulus $k_BT\gamma$ can be estimated via

$$\gamma = \frac{\langle L \rangle}{\langle \Delta L \rangle^2} \tag{9}$$

with $\Delta L = L - \langle L \rangle$ being the mean deviation from the average contour length of the fiber (defined as the length of the fiber axis $L = \Sigma_{i=1}^{N-N_c} |\vec{c}_{i+1} - \vec{c}_i|$). It should be noted that depending on $N_c$, the estimated values of the contour length, persistence length, and stretching modulus vary. In the case of $N_c$ being too large, the stretching modulus is underestimated because bending fluctuations within $i$ and $i+N_c$ are averaged out so that the contour length of the fiber appears to be smaller. On the other hand, values of $N_c$, which are too small lead to a helicoidal fiber axis, and the contour length of the fiber is overestimated. This entails a systematic error that must be minimized. We found that values of $N_c$ corresponding to one or two helical turns lead to reasonable estimates.

## III. RESULTS

In order to quantify the influence of the nucleosome excluded volume on the fiber stiffness, we performed a series of simulations with purely repulsive interactions between the nucleosome core particles, constant linker geometry, and variable core particle size. The lhs of Fig. 2 shows our results for the persistence length for two fiber geometries; the corresponding snapshots in the rhs of the figure illustrate the observed fiber stiffening with increasing core particle size.

To be more specific, we studied two different sets of angles, namely $\theta=145°$ and $\phi=100°$ as well as $\theta=90°$ and $\phi=100°$. In both cases, starting at $h=0$ (i.e., no nucleosomes present) we observe the theoretically expected values for the persistence length of the linker backbone [Eq. (97) in Ref. [23]], namely $l_p \simeq 14$ nm and $l_p \simeq 34$ nm, respectively. We verified this formula also for many other values of $\theta$ and $\phi$ (data not shown). However, with increasing $h$ the value of $l_p$ increases and reaches values of 240 nm and 90 nm, respectively, at the canonical value of $h=6$ nm. This corresponds to a 17-fold and threefold increase, respectively, of the fiber stiffness relative to the theoretical prediction. The different degrees of stiffness (and stiffening) directly reflect the different nucleosome densities in the two cases: in the $\theta=145°$-fiber the nucleosomes are always quite close to each other whereas the $\theta=90°$-fiber is still much more open.

We also performed simulations of stretched fibers with $\theta=145°$ and $\phi=110°$. The resulting force-elongation curves (red symbols in Fig. 3) and histograms of the end-to-end distance distribution (red symbols in Fig. 4) show the typical behavior of extensible wormlike chains. The entropic small force regime is strongly suppressed, since the $f=0$ contour length, $L=85$ nm, of fibers containing 50 nucleosomes is much smaller than their persistence length of $l_p=220$ nm. The effective stretching modulus $\gamma=8$ nm$^{-1}$ at finite extensions is smaller than the value $\gamma=14$ nm$^{-1}$ deduced from the analysis of the length fluctuations [see Eq. (9)] and larger than the theoretical prediction $\gamma=3$ nm$^{-1}$, which is based on the linker mechanics alone.

For our study of the effect of attractive interactions between core particles we focused on linker backbone geometries, which by themselves already lead to relatively dense fibers ($\theta=145°$ and $\phi=110°$). As a consequence, the local fiber geometry remains basically unchanged when we vary the strength of the attractive interaction from $\epsilon=0$ (the case of purely repulsive interactions discussed above) to $\epsilon=4$. For example, the observed attraction induced reductions in the fiber contour lengths are only on the order of 10%.

Weak attraction up to $\epsilon=2k_BT$ (green symbols in Figs. 3 and 4) has only a small effect on the observed fiber properties. While the contour length decreases to about $L=80$ nm, there is a corresponding small increase in both the fiber stiffness and its stretching modulus, yielding an overall small increase in the end-to-end distance. The situation changes dramatically for larger values of the attractive well depth. In the absence of external forces fibers with $\epsilon=3k_BT$ and, in particular, with $\epsilon=4k_BT$ (blue/magenta symbols in Figs. 3 and 4) have considerably smaller and more broadly distributed end-to-end distances $R_E$. For small forces the $\epsilon=4k_BT$ fiber shows a quasiplateau in the force-extension curve.

The origin of this peculiar behavior can be identified by inspecting snapshots of the $\epsilon=4k_BT$ fiber (Fig. 3): At $f=0$ pN the fiber forms a hairpin structure where the end nucleosomes (in red) are located at the same end of the structure. The hairpin persists at $f=0.5$ pN, but opens up into a straight configuration around $f=2$ pN. For larger forces all

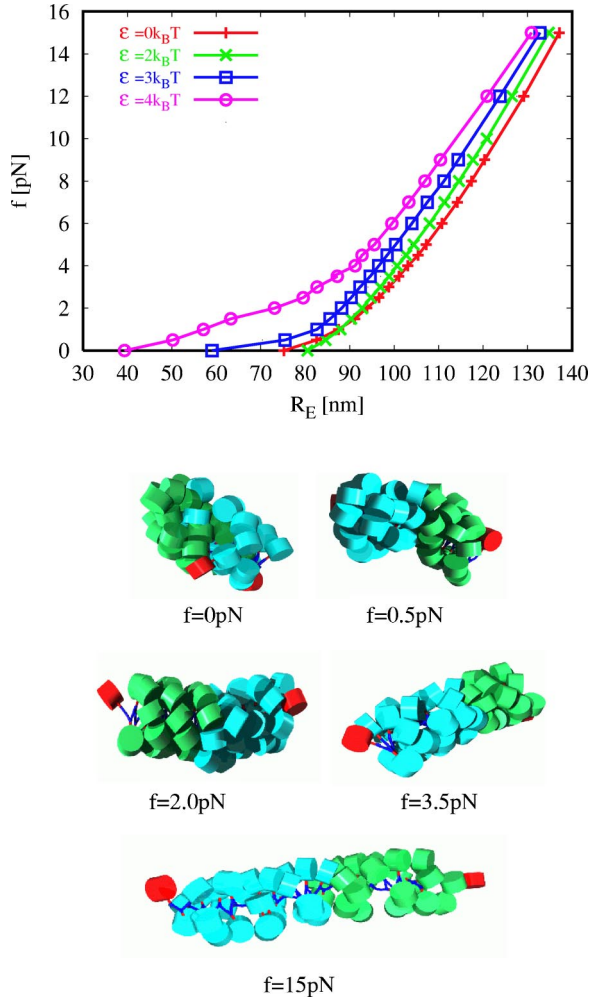


FIG. 3. Force-extension curves for fibers with $\theta=145°$, $\phi=110°$, and $B=7.14$ nm. The curves correspond to fibers with different nucleosomal attraction, namely $\epsilon=0$ (pure hardcore) and $\epsilon=2$, 3, $4k_BT$. At $\epsilon=4k_BT$ occurs a force plateau around $2pN$. Snapshots of fibers with $\theta=145°$, $\phi=110°$, and $B=7.14$ nm at different stretching forces for $\epsilon=4k_BT$. To facilitate the detection of hairpins, one half of the chain is shown in green while the other half is shown in cyan. The end nucleosomes are labeled red. The fiber at $f=0$ pN shows a kink close to the center of the chain. Up to $f=2$ pN the kink is still present, but the ends get pulled out. For $f=15$ pN the fiber is stretched and nucleosomal contacts are broken.

observed force elongation curves show qualitatively the same WLC behavior.

## IV. DISCUSSION

Our results show that the properties of dense chromatin fibers are dominated by the interactions between the nucleosome core particles, while the mechanical properties of the linker backbone play a less important role. The dominant effect of excluded volume interactions is to stiffen the fiber. The persistence lengths of the order of 200–250 nm observed in the present study are in good agreement with the values obtained by Münkel and Langowski [27] and Wedemann and Langowski [28]. The surprising result of our simulations is that attractive interactions of a few $k_BT$ per nucleosome pair are sufficient to bend fibers with a contour length of about 1/3 of the persistence length into dense hairpin configurations. Judging from Fig. 5 in Ref. [20], hairpins also occurred in the simulations by Katritch, Bustamante, and Olson—even though the authors did not discuss this issue in their paper. Since the observed force-elongation

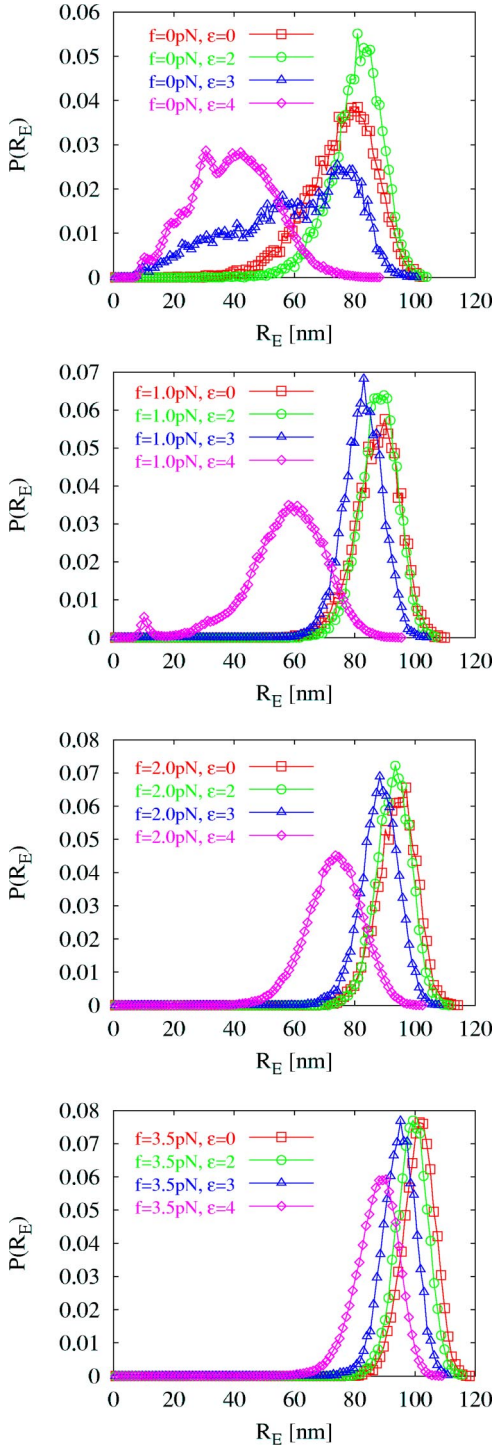


FIG. 4. Probability density of the end-to-end distance $R_E$ of a fiber with $\theta=145°$, $\phi=110°$, and $B=7.14$ nm for various GB energy well depths $\varepsilon$ and stretching forces $f$ as specified in the legends. See text for details.

curves show qualitatively similar features in all three cases, it is tempting to speculate that similar effects also occurred in the stretching experiment by Cui and Bustamante [18]. In the following, we will discuss the condensation of semiflexible filaments, the local structure of the hairpins observed in our simulations, the signature of hairpin opening in stretching experiments, and possible implications of our observations for the folding of chromatin into chromosomes.

### A. Condensation of semiflexible filaments

The condensation of semiflexible filaments due to short-range attractive interactions has recently been treated in detail by Schnurr, Gittes, and MacKintosh [44]. They introduced a *condensation length* $L_c=\sqrt{k_BTl_p/\sigma_{attr}}$ ($\sigma_{attr}$: attraction energy per) by balancing expressions for typical bending and surface energies $k_BTl_p/L\sim\sigma_{attr}L$. Filaments with a contour length $L/L_c<\mathcal{O}(10)$ remain extended, while longer chains aggregate into structures with a typical size of the order of $L_c$. So-called racquet states consist of a straight stem where the chain is folded back on itself several times and where 180° U-turns are shaped like the head of a tennis racquet. A racquet state with one turning point resembles our hairpin structure. Longer fibers lower their energy by having multiple turning points. For infinitely thin filaments Schnurr, MacKintosh, and Williams were able to show that the kinetically preferred racquet states [45] have slightly higher energies than toroidal structures.

In the present case, we measured a typical attraction energy per length of $\sigma_{attr}\approx(3/4)k_BT$ nm$^{-1}$ for hairpin conformations of the $\epsilon=4k_BT$-fiber in good agreement with an estimate of $\epsilon/h=4k_BT/6$ nm for the attractive energy per nucleosome pair of height $h$. Using this estimate and a persistence length $l_p=240$ nm, chromatin fibers with weak attractive interactions should start to condense, if they are longer than about $\mathcal{O}(10)L_c\approx\sqrt{k_BT/\epsilon}$ 400 nm. Note that the above argument breaks down for $\epsilon>6k_BT$, when the predicted racquet head or torus radii become smaller than the radius of the 30-nm fiber.

Can the structure of the hairpins we observe really be understood in the framework of the WLC model? Or does one have to consider the relatively sharp turning points with the curvature radii of the order of the fiber radius as localized kink defects? Following the analysis of Schnurr, Gittes, and MacKintosh [44], the fibers in our simulations are too short to fold back on themselves. The WLC estimate of the bending energy for a U-turn with radius 15 nm is $U_{kink}\approx25k_BT$, while the onset of hairpin formation at $\epsilon=3k_BT$ in 80-nm-long fibers suggest that the actual energy penalty for the kinks is as small as $U_{kink}\approx9k_BT$. We note that the combination of finite fiber radii and relatively small kink energies should stabilize racquet structures relative to toroids.

### B. Hairpin structure

The internal structure of hairpin configurations shows up very clearly in the contact matrix $\mathcal{M}_{\text{contact}}$ of the fiber that we depict in Fig. 5. For a given configuration the contact matrix is defined as follows: If a pair of nucleosomes $i$ and $j$ is in contact (center-to-center distance smaller than $1.5d=15$ nm) one has $\mathcal{M}^{(ij)}_{\text{contact}}=1$, otherwise $\mathcal{M}^{(ij)}_{\text{contact}}=0$. By taking the average of the matrix elements for many configurations of a given simulation run, we obtain 2D histograms as is shown in Fig. 5. For large forces no kinks are present and the nucleosomes of the fiber form a quite regular crossed-linker structure. We find two pronounced diagonals at the positions $i=j\pm2$ that correspond to "short-ranged" excluded volume interaction. Less-pronounced side stripes parallel to the main diagonal are also observed and describe interactions between nucleosomes of neighboring turns, especially at $i=j\pm5$ and at $i=j\pm7$. Hairpins manifest themselves by crosslike patterns in the contact matrices with branches along the secondary diagonal. The location of the kink corresponds to the point where the two diagonals cross each other. Closer inspection of the histograms shows that the hairpin arms outside the kink region are partially interdigitated, but not strongly perturbed. However, the effect is strong enough to effectively prevent any possibility of sliding of the two arms with respect to each other on the time scale of our simulations. Therefore, a hairpin structure, once formed, can be very stable with a frozen in position of the turning point. With respect to the fiber structure at the turning point, Fig. 5(d) in particular shows disruptions of the internal order of the nucleosomes: The diagonals $i=j\pm2$ are broken at that position, presumably due to broken contacts of nucleosomes located at the outside of the turning point. This observation supports the picture of a localized kink defect.

### C. Large scale versus local decondensation in stretching experiments

Toroidal or racquetlike condensates become unstable under the influence of a stretching force, if the applied force $f$ exceeds a value on the order of the attractive energy per unit length $\sigma_{attr}$. Neglecting kinetic barriers (for a discussion of DNA unwrapping from nucleosomes or toroidal aggregates see [46]), the corresponding force plateau in the force-extension curves for chromatin fibers should be observed for forces of $f\approx\sigma_{attr}\approx(2/3)(\epsilon/k_BT)$pN. In order to experimentally distinguish this scenario from local structural changes that are expected to occur at similar force levels [13], one should plot force-*relative* extension curves for fibers reconstituted under similar conditions on DNA strands of different length. In the case of local structural changes, the obtained curves coincide, while for a global decondensation the size of the unperturbed state is of order $L_c$ independently of the fiber length.

### D. Biological implications

As a final point we discuss possible biological implications of fiber stiffening and hairpin formation. Both effects are associated with characteristic length scales; fiber stiffening with a persistence length on the order of 300 nm, hairpin formation with a condensation length on the order of a few tens of nm.

We note again that the biochemical control of the effective interaction between nucleosomes is essential for the con-

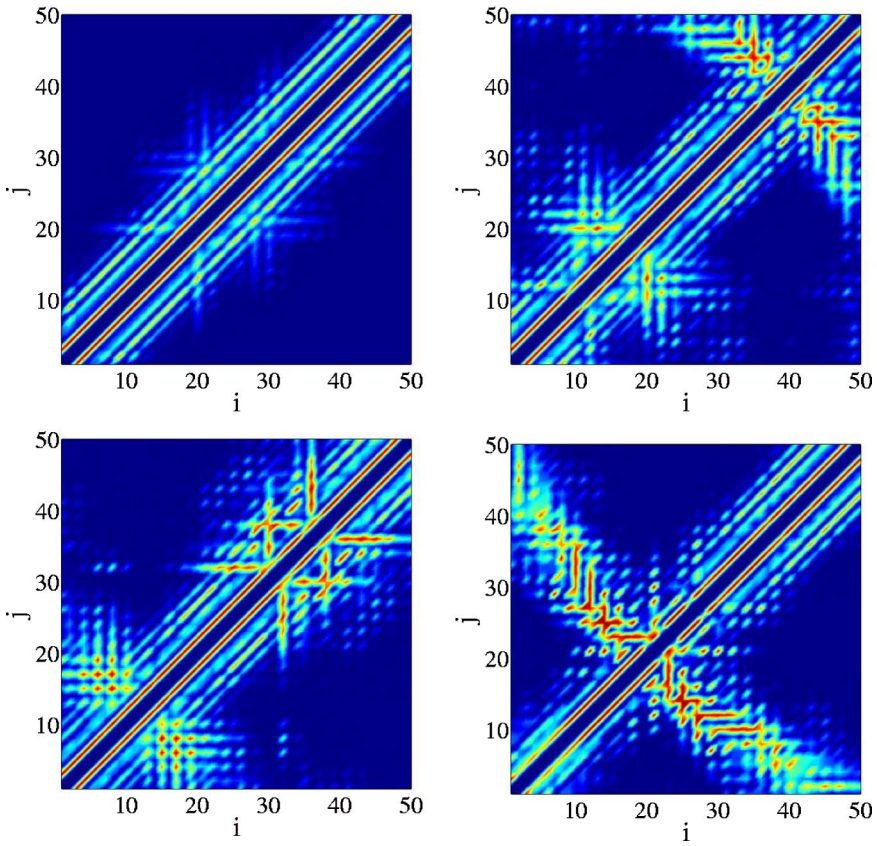


FIG. 5. Contact matrix of the fiber with $\epsilon = 4\ k_B T$, $\theta = 145°$, $\phi = 110°$, and $B = 7.14$ nm. (a) At an external tension $f = 3.5$ pN the fiber is stretched and there is no hairpin. (b)–(d) Without an external force, $f = 0$ pN, one can clearly detect hairpin structures. The simulation runs (b) and (c) show the occurrence of two hairpins, whereas in (d) only one hairpin can be identified.

densation and decondensation of chromosomes during the cell cycle [47]. There is indirect experimental evidence for the formation of chromosomal DNA loops having a size of about 50 kilobases [48] (corresponding to about 250 nucleosomes), e.g., from the comparison of separation patterns of excised large DNA fragments by pulsed field electrophoresis with the patterns obtained by DNA cleavage by topoisomerase II of the nuclear matrix of the cell [49,50]. Using a nucleosome density of $6/(11\ \text{nm})$, 250 nucleosomes correspond to a fiber length of 460 nm, i.e., about twice the persistence length of 240 nm found in our simulations.

There are two scenarios linking the persistence length to the loop size; both are based on the observation that the free energy cost for the formation of a loop is smallest for semiflexible chains with a length of about twice the persistence length. For shorter chains the bending energy is high; for larger chains the entropy of chain conformations counteracts the loops formation. In the first (equilibrium) scenario, the chromatin fiber loops around strongly attracting organizing centers. Spherical centers could induce the formation of rosette structures [51]. Filamentous organizing centers could lead to structures resembling cartoons of chromosomes often found in biological textbooks, cf., e.g., Ref. [52]. The second scenario, which links the persistence length to the loop size, is closer to what we observed in our simulations: if the attraction between fibers is strong enough to prevent structural reorganization after the two halves of the fiber have tightly closed the gap between the point of first contact and the hairpin defect, then loops with the typical size of the fiber persistence length are preferred for kinetic reasons. Hairpins have indeed been observed in cryo-EM pictures of chromatin fibers in the presence of myeloid and erythroid nuclear termination stage-specific protein (MENT) [53], a protein that is involved in the formation of dense, transcriptionally inert sections of chromatin, the so-called heterochromatin.

If, on the other hand, structural reorganization is still possible in collapsed fibers, then the size of the aggregates should be controlled by the smaller condensation length and not by the persistence length of the 30-nm fiber. Fibers with diameters ranging between 60 to 130 nm diameter have indeed been observed in mitotic and in G1 chromosomes and are called chromonema fibers [54], cf., also Ref. [47]. However, the folding of 30-nm fibers into superfibers with a diameter on the order of the condensation length requires a mechanism that prevents the formation of globular aggregates.

## V. CONCLUSION

We have used computer simulations of model chromatin fibers to investigate the influence of excluded volume and attractive interactions between the nucleosomes on the large-scale structure and elasticity of the 30-nm chromatin fiber. Our results shed light (i) on the discrepancy between the theoretically expected and the observed persistence length of 200-300 nm as well as (ii) on the somewhat counterintuitive observation that such fibers nevertheless seem to be able to curl up into chromonema fibers with diameters of 60–130 nm.

Our results clearly show that the stiffness of dense fibers is dominated by excluded volume interactions between nucleosomes. The observed persistence lengths exceed estimates based on the linker backbone elasticity by one order of magnitude. With respect to internucleosomal attraction, we have concentrated on generic, nonlocal aspects of fiber condensation. The 2 pN force plateau observed in our simulations reflects a structural feature *beyond* the 30-nm fiber: the opening of a hairpin. Our results suggest that aligned (anti-) parallel fibers are only weakly perturbed, but that the fiber geometry is locally disrupted at the 180° turning point. The crucial point is that the energetic cost of this localized defect is considerably smaller than for a smoothly bending semiflexible filament with the same bending persistence length as chromatin. This effect could be important for an understanding of chromatin folding in chromosomes.

## ACKNOWLEDGMENTS

We thank K. Kremer, I. M. Kulic, J. Langowski, and J. Widom for valuable discussions and M. R. Ejtehadi for providing parts of the simulation code. B.M. and R.E. gratefully acknowledge financial support from an Emmy-Noether grant of the DFG.

[1] K. E. van Holde, *Chromatin* (Springer, New York, 1989).
[2] F. Thoma, T. Koller, and A. Klug, J. Cell Biol. **83**, 404 (1979).
[3] J. Widom, J. Mol. Biol. **190**, 411 (1986).
[4] J. Bednar *et al.*, Proc. Natl. Acad. Sci. U.S.A. **95**, 14173 (1998).
[5] K. Luger, A. W. Mader, R. K. Richmond, D. F. Sargent, and T. J. Richmond, Nature (London) **389**, 251 (1997).
[6] J. Widom, Annu. Rev. Biophys. Biophys. Chem. **18**, 365 (1989).
[7] K. V. Holde and J. Zlatanova, J. Biol. Chem. **270**, 8373 (1995).
[8] K. V. Holde and J. Zlatanova, Proc. Natl. Acad. Sci. U.S.A. **93**, 10548 (1996).
[9] J. Langowski and H. Schiessel, in *Chromatin Structure and Dynamics: State-of-the-Art*, edited by J. Zlatanova and S. H. Leuba, New Comprehensive Biochemistry Vol. 39 (Elsevier, New York, 2004), p. 397.
[10] J. T. Finch and A. Klug, Proc. Natl. Acad. Sci. U.S.A. **73**, 1897 (1976).
[11] J. Widom and A. Klug, Annu. Rev. Biophys. Biophys. Chem. **43**, 207 (1985).
[12] C. L. Woodcock, S. A. Grigoryev, R. A. Horowitz, and N. Whitaker, Proc. Natl. Acad. Sci. U.S.A. **90**, 9021 (1993).
[13] H. Schiessel, W. M. Gelbart, and R. Bruinsma, Biophys. J. **80**, 1940 (2001).
[14] J. Bednar, R. A. Horowitz, J. Dubochet, and C. L. Woodcock, J. Cell Biol. **131**, 1365 (1998).
[15] S. H. Leuba *et al.*, Proc. Natl. Acad. Sci. U.S.A. **91**, 11621 (1994).
[16] J. Zlatanova, S. H. Leuba, and K. van Holde, Biophys. J. **74**, 2554 (1998).
[17] S. E. Gerchman and V. Ramakrishhnan, Proc. Natl. Acad. Sci. U.S.A. **84**, 7802 (1987).
[18] Y. Cui and C. Bustamante, Proc. Natl. Acad. Sci. U.S.A. **97**, 127 (2000).
[19] J. Zlatanova and S. H. Leuba, J. Mol. Biol. **331**, 1 (2003).
[20] V. Katritch, C. Bustamante, and W. K. Olson, J. Mol. Biol. **295**, 29 (2000).
[21] E. Ben-Haim, A. Lesne, and J.-M. Victor, Phys. Rev. E **64**, 051921 (2001).
[22] E. Ben-Haim, A. Lesne, and J.-M. Victor, Physica A **314**, 592 (2002).
[23] H. Schiessel, J. Phys.: Condens. Matter **15**, R699 (2003).
[24] K. van Holde and J. Zlatanova, J. Mol. Biol. **93**, 8373 (1995).
[25] J. Yao, P. T. Lowary, and J. Widom, Proc. Natl. Acad. Sci. U.S.A. **87**, 7603 (1990).
[26] P. J. G. Butler and J. O. Thomas, J. Mol. Biol. **281**, 401 (1998).
[27] C. Münkel and J. Langowski, Phys. Rev. E **57**, 5888 (1998).
[28] G. Wedemann and J. Langowski, Biophys. J. **82**, 2847 (2002).
[29] C. Bustamante, S. B. Smith, J. Liphardt, and D. Smith, Curr. Opin. Struct. Biol. **10**, 279 (2000).
[30] J. Widom, Proc. Natl. Acad. Sci. U.S.A. **89**, 1095 (1992).
[31] R. Everaers and H. Schiessel (unpublished).
[32] J.-L. Barrat and J.-F. Joanny, Adv. Chem. Phys. **94**, 1 (1996).
[33] H. Schiessel, Europhys. Lett. **58**, 140 (2002).
[34] S. Mangenot, A. Leforestier, P. Vachette, D. Durand, and F. Livolant, Biophys. J. **82**, 345 (2002).
[35] S. Mangenot, E. Raspaud, C. Tribet, L. Belloni, and F. Livolant, Eur. Phys. J. E **7**, 221 (2002).
[36] R. Podgornik, J. Chem. Phys. **118**, 11286 (2003).
[37] F. Mühlbacher, C. Holm, and H. Schiessel (unpublished).
[38] D. A. Beard and T. Schlick, Structure (London) **9**, 105 (2001).
[39] A. Leforestier and F. Livolant, Biophys. J. **73**, 1771 (1997).
[40] R. Berardi, C. Fava, and C. Zannoni, Chem. Phys. Lett. **297**, 8 (1998).
[41] R. Everaers and M. R. Ejtehadi, Phys. Rev. E **67**, 041710 (2003).
[42] B. Mergell, M. R. Ejtehadi, and R. Everaers, Phys. Rev. E **68**, 021911 (2003).
[43] N. Metropolis, A. W. Rosenbluth, M. N. Rosenbluth, A. N. Teller, and E. Teller, J. Chem. Phys. **21**, 1087 (1953).
[44] B. Schnurr, F. Gittes, and F. C. MacKintosh, Phys. Rev. E **65**, 061904 (2002).
[45] B. Schnurr, F. C. MacKintosh, and D. R. M. Williams, Europhys. Lett. **51**, 279 (2000).
[46] I. M. Kulic and H. Schiessel, Phys. Rev. Lett. **92**, 228101 (2004).
[47] P. J. Horn and C. L. Peterson, Science **297**, 1824 (2002).
[48] C. R. Calladine and H. R. Drew, *Understanding DNA: The Molecule and How It Works* (Academic, New York, 1999).
[49] M. A. Lagarkova, O. V. Iarovaia, and S. V. Razin, J. Biol. Chem. **270**, 20239 (1995).
[50] I. I. Gromova, B. Thomsen, and S. V. Razin, Proc. Natl. Acad.

Sci. U.S.A. **92**, 102 (1995).
[51] H. Schiessel, J. Rudnick, R. Bruinsma, and W. M. Gelbart, Europhys. Lett. **51**, 237 (2000).
[52] B. Alberts *et al.*, *Molecular Biology of the Cell* (Garland, New York, 1994).
[53] S. A. Grigoryev, J. Bednar, and C. L. Woodcock, J. Biol. Chem. **274**, 5626 (1999).
[54] A. S. Belmont and K. Bruce, J. Cell Biol. **127**, 287 (1994).